Transport and Communications Science Journal

NONLINEAR INTERFACIAL CONTACT LAWS IN MULTI-LAYER ELASTIC-VISCOELASTIC STRUCTURAL SYSTEMS

Tran Nam Hung [*], Nguyen Thi Thu Nga

Le Quy Don Technical University, No 236, Hoang Quoc Viet Street, Hanoi, Vietnam

ARTICLE INFO

[*] *Corresponding author*

Email: tranhung@lqdtu.edu.vn

Abstract. Layered structures are widely used in construction, such as pavement structures consisting of multiple layers of different materials or interfaces between bricks and mortar in masonry structures, etc. In analyzing such structures, understanding the properties of the interface between two layers of materials is essential. If one layer of material contains cracks and layers exhibit viscoelastic behavior, determining the properties of the interface becomes challenging. This study proposes a constitutive mechanical law to model the behavior of the interface between a microcracked viscoelastic medium and an undamaged elastic body based on the homogenization method. The interface is modeled by a layer of zero thickness. The coupling between the homogenization technique and the Griffith's theory is used to provide the effective behavior of the micro-cracked medium. The interface is modelled as an effective medium (EF) characterized by normal and tangential stiffnesses (C_N, C_T). In this work, two viscoelastic models are considered, i.e., Burger and Modified Maxwell. The formulas of C_N and C_T for two cases of crack distributions (isotropic and transversely isotropic) are obtained by asymptotic techniques where the thickness of the joint tends to zero.

Keywords: Nonlinear interfacial laws, homogenization, micro-crack, viscoelastic.

@ 2024 University of Transport and Communications

1. INTRODUCTION

Recently, in civil engineering practice, growing numbers of hybrid structures made from different materials have been built. These structures are widely employed in the construction of road pavement surfaces, embankments, and civil engineering projects. Understanding the characteristics of interactions between material layers is essential for more accurately simulating the behavior of hybrid structures under the influence of various load types. These materials (steel, concrete, asphalt concretes, masonry, glass, …) may work integrated or jointly resulting in substantial savings and higher quality constructions [1-3]. Indeed, structural interaction between the components of hybrid structures produces a composite structure with a complicated behavior and depends on the type of the components [4-6]. When one material is much stiffer than the other, the phenomenon of delamination causes complex degradations of layers and inter-laminar connections. The more solid material is usually assumed to be an undamaged elastic part while the weaker one is usually a nonlinear material [7]. It is well known that cracks or debonding usually run along the interface [8-10] and material properties of the matrix, i.e., the weaker, play a very important role [11]. Experimental outcomes confirmed that most of the interface between a linear material and a nonlinear material behaves nonlinearly [12,13]. Besides, among the hybrid structures, concrete, and mortar, which exhibit usually viscoelastic behavior, are the most commonly used materials [14,15]. Although extensive research has been done into hybrid structures, little attention has been paid to discrete interface connections between their components, especially in the case of nonlinear behavior interfaces. Indeed, the interface is assumed to be elastic and damageable in most cases [16-18]. Some studies analyze crack growth along the interface [19,20]. Reinoso et al. [21] proposed a nonlinear cohesive interface model with a finite thickness for modeling delamination in fiber-reinforced composite laminates relying on the solid shell concept which is especially relevant for the analysis of thin-walled composite structures.

This study aims at deriving nonlinear laws, based on homogenization methods, for the interface between a viscoelastic medium and an undamaged elastic body. The interface is represented by a layer of zero thickness with a low stiffness and characterized by normal and tangential stiffnesses (C_N, C_T). Rekik and Lebon [18] proposed a homogenization procedure to obtain an interface law for the case of a masonry structure composed of bricks and mortar. They assumed that the interface material is a third material, which is a mixture of the two materials with the presence of microcracks. The effective behavior of this interface material is estimated by the Kachanov homogenization model. Then, the normal and tangential rigidities of this interface are defined by using the asymptotic analysis technique where the thickness tends to zero. This procedure is only good if the volume fractions of two material components (bricks and mortar) are equal and their mechanical properties are not much different.

This study aims to propose rheological laws for the interface between two materials of hybrid structures that the difference in stiffness between them is important. When one material is much more solid than the other, the interface law is assumed to depend only on the weaker component. This component is proposed to have viscoelastic behavior with or without micro-cracks. These features of the hybrid structural behavior suggested the use of non-linear interface elements. The mechanical characteristic of the micro-cracked viscoelastic medium is investigated by using the coupling between the homogenization technique and Griffith's theory. The steps are illustrated in Figure 1. Two types of viscoelastic models, Burger and Modified Maxwell are adopted for isotropic and transversely isotropic

cases. After an effective medium (EM) is defined, the interface law is derived by an asymptotic analysis. The properties of the interface law will be discussed in the third part.
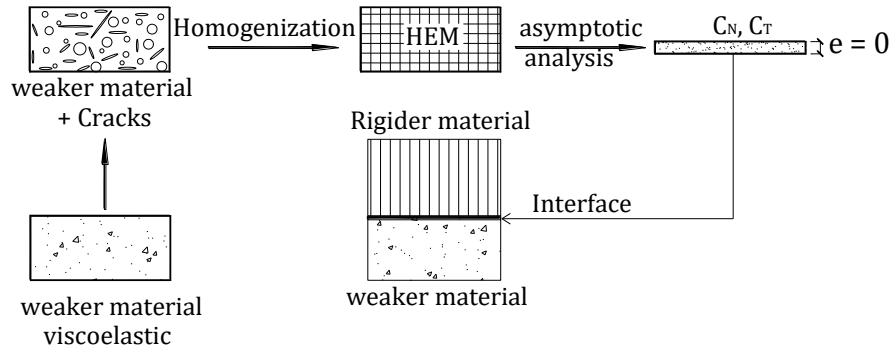
Figure 1. Homogenization methods for nonlinear interfacial laws.

2. COUPLING BETWEEN HOMOGENIZATION AND GRIFFITH THEORY

To describe the viscoelastic behavior of an intact medium at ambient temperature, several rheological models have been proposed, such as Maxwell, Kelvin-Voigt, Ross, Burgers, Maxwell modified, Maxwell generalized, Kelvin-Voigt generalized, and USBR [22, 23]. The Modified Maxwell model has been proposed by Lenczner [24] and Choi et al. [25] to model the creep behavior of masonry while the Burgers model provides good results for concrete behavior [26]. Therefore, only the Burgers and Modified Maxwell (MM) models are considered in this work for most of the hybrid structures.

The macroscopic strain is deduced from the average of the local strain $\varepsilon(t)$ in the uncracked medium corrected by the strain induced by the presence of micro-cracks:

$$\bar{\varepsilon} = \frac{1}{V}\left(\int_{\Omega_s} \varepsilon dV + \sum_i \int_{C_i} [u_i] \otimes^s n_i dS\right) \tag{1}$$

where Ω_s is the domain occupied by the uncracked material, V is the volume of Ω (with or without cracks) and $a \otimes^s b = \dfrac{a \otimes b + b \otimes a}{2}$ for the vectors a and b, C_i and n_i denote respectively the area of the crack i and the normal vector to the plane of this crack, $[u_i]$ denotes the displacement jump across crack i.

To estimate the effective behavior of the viscoelastic medium containing an isotropic or parallel distribution of elliptic fissures, three steps are proposed as follows:

• The 1st step consists of the passage from the space of real times to the symbolic space. This makes it possible to convert a problem of linear viscoelastic material into a symbolic linear elastic problem due to the Laplace-Carson (LC) transform. In the symbolic space, the displacement jumps $[u_i]^*$ are supposed to depend linearly on the macroscopic stress and are expressed by the coupling between the diluted homogenization scheme and the Griffith theory. Concretely, in mode I the displacement jump is normal to the crack plane $[u_n]^*$ and in mode II the displacements jump is parallel to the crack plane $[u_t]^*$

$$[u_n]^* = \frac{4(1-v_s^*)}{\pi}\frac{\Sigma^*}{\mu_s^*}\sqrt{l^2-\rho^2}; \; [u_t]^* = \frac{4(1-v_s^*)}{\pi(2-v_s^*)}\frac{\Sigma^*}{\mu_s^*}\sqrt{l^2-\rho^2} \tag{2}$$

The equation (1) can be rewritten as follows:

$$\overline{\varepsilon}^* = \frac{1}{V}\left(\int_{\Omega_s}\varepsilon^* dV + \sum_i \int_{C_i}[u]_i^* \otimes^s n_i dS\right) \tag{3}$$

- The 2nd step deduces the macroscopic symbolic deformation of the medium. It is possible to define an effective linear behavior for the micro-cracked medium in the symbolic space in equation (3) as follows:

$$\overline{\varepsilon}^* = C_{d_c}^{*-1} : \Sigma^* \tag{4}$$

where $C_{d_c}^{*-1} = S_{d_c}^*$ is the apparent effective compliance tensor, $C_{d_c}^*$ is the apparent effective stiffness tensor of the micro-cracked viscoelastic medium.

- The 3rd step is to determine the global behavior in the real space time. The inverse of the LC transform is only possible for some simple cases. Thus, it is then interesting to approach in the symbolic space, at least in the short and long terms, the symbolic effective stiffness (or compliance) by an existing rheological model. For example, if the uncracked medium behaves as the MM model, we try to approach the symbolic effective behavior of the corresponding micro cracked medium by the same model. The best approximation of the apparent rigidity $C_{d_c}^*$ which results from the coupling between the homogenization technique and Griffith's theory of a micro- cracked viscoelastic mortar whose creep behavior follows the rheological model of MM in the class of the same model (i.e., of MM) in short (t → 0) and long (t → ∞) terms (for more details, see [27, 28]). After validation of this approximation in short and long terms, the inversion of the apparent effective stiffness will be straightforward. Therefore, the effective behavior of the micro-cracked viscoelastic mortar could be expressed in the real space time.

Hooke's Law provides the following definition of the compliance tensor of homogenized effective medium:

$$S = \begin{bmatrix} \dfrac{1}{\tilde{E}_1} & -\dfrac{\tilde{v}_{21}}{\tilde{E}_1} & -\dfrac{\tilde{v}_{31}}{\tilde{E}_3} & 0 & 0 & 0 \\[3mm] -\dfrac{\tilde{v}_{12}}{\tilde{E}_1} & \dfrac{1}{\tilde{E}_1} & -\dfrac{\tilde{v}_{31}}{\tilde{E}_3} & 0 & 0 & 0 \\[3mm] -\dfrac{\tilde{v}_{13}}{\tilde{E}_1} & -\dfrac{\tilde{v}_{13}}{\tilde{E}_1} & \dfrac{1}{\tilde{E}_3} & 0 & 0 & 0 \\[3mm] 0 & 0 & 0 & \dfrac{1}{\tilde{\mu}_{23}} & 0 & 0 \\[3mm] 0 & 0 & 0 & 0 & \dfrac{1}{\tilde{\mu}_{23}} & 0 \\[3mm] 0 & 0 & 0 & 0 & 0 & \dfrac{2(1+\tilde{v}_{12})}{\tilde{E}_1} \end{bmatrix} \tag{5}$$

The stiffness tensor C is the inverse of S. If $\tilde{C}_{3333}$, $\tilde{C}_{1313}$ are the components of $\square$, then

$$\tilde{C}_{3333} = \tilde{E}_3, \ \tilde{C}_{1313} = \tilde{\mu}_{23} \qquad (6)$$

An effective medium of the viscoelastic medium with opening spherical cracks is shown in the following for two cases of crack distribution: isotropy and parallel.

2.1. Isotropic distribution of cracks

For the case of isotropic distribution of cracks, the apparent effective stiffness of the micro-cracked viscoelastic medium is also isotropic and can be expressed in the tensor form as:

$$C^*_{d_c} = 3\tilde{k}^*_{d_c} J + 2\tilde{\mu}^*_{d_c} K \qquad (7)$$

with $\tilde{k}^*_{d_c}$ and $\tilde{\mu}^*_{d_c}$ are the apparent effective bulk and shear moduli, respectively given by:

$$\frac{1}{\tilde{k}^*_{d_c}} = \frac{1 + d_c Q^*}{k^*_s}, \quad \frac{1}{\tilde{\mu}^*_{d_c}} = \frac{1 + d_c M^*}{\mu^*_s} \qquad (8)$$

where $Q^* = \dfrac{16}{9} \dfrac{1 - \nu_s^{*2}}{1 - 2\nu_s^*}, M^* = \dfrac{32}{45} \dfrac{(1 - \nu_s^*)(5 - \nu_s^*)}{1 - 2\nu_s^*}$ and $d_c = Na^3$ is the dimensionless crack density parameter; N is the number of cracks per unit of volume and a is radius of the cracks.

2.1.1 Burger model
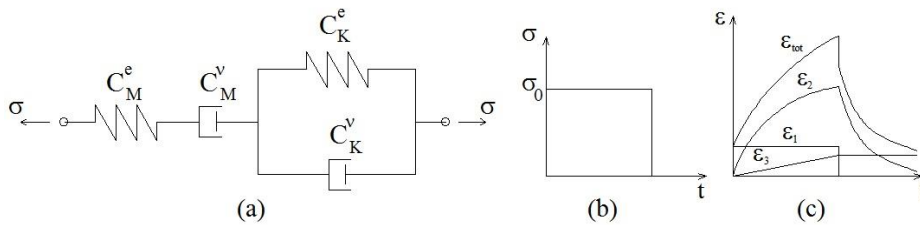
Figure 2. Burger model (a) and its deformation response (c) under the effect of a constant stress (b).

Nguyen et al. [26] showed that the Burger model is the best approximation to identify the apparent rigidity $S^*_{d_c} = C^{*^{-1}}_{d_c}$ for micro-cracked viscoelastic concrete. In such a model, two moduli in (7) are:

$$\begin{cases} \dfrac{1}{\tilde{k}^*_{Bu}(p, d_c)} = \dfrac{1}{k^e_M(d_c)} + \dfrac{1}{p\eta^s_M(d_c)/3} + \dfrac{1}{k^e_K(d_c) + p\eta^s_K(d_c)/3}; \\ \dfrac{1}{\tilde{\mu}^*_{Bu}(p, d_c)} = \dfrac{1}{\mu^e_M(d_c)} + \dfrac{2}{p\eta^d_M(d_c)} + \dfrac{1}{\mu^e_K(d_c) + p\eta^d_K(d_c)/2} \end{cases} \qquad (9)$$

which are the functions of 8 parameters:

$$\begin{cases} \dfrac{1}{k^e_M(d_c)} = \dfrac{1 + Q^e_M d_c}{k^e_M}, \dfrac{1}{\mu^e_M(d_c)} = \dfrac{1 + M^e_M d_c}{\mu^e_M}, \dfrac{1}{\eta^s_M(d_c)} = \dfrac{1 + Q^v_M d_c}{\eta^s_M}, \dfrac{1}{\eta^d_M(d_c)} = \dfrac{1 + M^v_M d_c}{\eta^d_M} \\ \dfrac{1}{k^e_K(d_c)} = \dfrac{1 + Q^e_K d_c}{k^e_K}, \dfrac{1}{\mu^e_K(d_c)} = \dfrac{1 + M^e_K d_c}{\mu^e_K}, \dfrac{1}{\eta^s_K(d_c)} = \dfrac{1 + Q^v_K d_c}{\eta^s_K}, \dfrac{1}{\eta^d_K(d_c)} = \dfrac{1 + M^v_K d_c}{\eta^d_K} \end{cases} \qquad (10)$$

where

$$
\begin{cases}
Q_M^e = Q_0^\infty = \dfrac{4}{3}\dfrac{k_M^e(3k_M^e+4\mu_M^e)}{\mu_M^e(3k_M^e+\mu_M^e)}, \quad Q_M^v = Q_0^0 = \dfrac{16}{9}\dfrac{\eta_M^s(\eta_M^s+2\eta_M^d)}{\eta_M^d(2\eta_M^s+\eta_M^d)} \\[2mm]
Q_K^e = Q_0^0 + \dfrac{3k_K^e}{\eta_M^s}Q_1^0 - \dfrac{k_K^e}{k_M^e}(Q_0^\infty - Q_0^0), \quad Q_K^v = Q_0^\infty + \dfrac{\eta_K^s}{3k_M^e}Q_{-1}^\infty - \dfrac{\eta_K^s}{\eta_M^s}(Q_0^0 - Q_0^\infty) \\[2mm]
Q_1^0 = \dfrac{32}{9}\dfrac{\eta_M^s}{\eta_M^d}\dfrac{(\eta_M^{s\,2}+\eta_M^s\eta_M^d+\eta_M^{d\,2})}{(2\eta_M^s+\eta_M^d)^2}\left[\dfrac{\eta_M^s}{3}\left(\dfrac{1}{k_M^e}+\dfrac{1}{k_K^e}\right)-\dfrac{\eta_M^d}{2}\left(\dfrac{1}{\mu_M^e}+\dfrac{1}{\mu_K^e}\right)\right] \\[2mm]
Q_{-1}^\infty = -\dfrac{4}{3}\dfrac{k_M^e}{\mu_M^e}\dfrac{(9k_M^{e\,2}+6\mu_M^e k_M^e+4\mu_M^{e\,2})}{(3k_M^e+\mu_M^e)^2}\left[3k_M^e\left(\dfrac{1}{\eta_M^s}+\dfrac{1}{\eta_K^s}\right)-2\mu_M^e\left(\dfrac{1}{\eta_M^d}+\dfrac{1}{\eta_K^d}\right)\right] \\[2mm]
M_M^e = M_0^\infty = \dfrac{16}{45}\dfrac{(9k_M^e+4\mu_M^e)}{(3k_M^e+\mu_M^e)}\dfrac{(3k_M^e+4\mu_M^e)}{(3k_M^e+2\mu_M^e)}, \; M_M^v = M_0^0 = \dfrac{32}{45}\dfrac{(\eta_M^s+2\eta_M^d)}{(\eta_M^s+\eta_M^d)}\dfrac{(3\eta_M^s+2\eta_M^d)}{(2\eta_M^s+\eta_M^d)} \\[2mm]
M_K^e = M_0^0 + \dfrac{2\mu_K^e}{\eta_M^d}M_1^0 - \dfrac{\mu_K^e}{\mu_M^e}(M_0^\infty - M_0^0), \; M_K^v = M_0^\infty + \dfrac{\eta_K^d}{2\mu_M^e}M_{-1}^\infty - \dfrac{\eta_K^d}{\eta_M^d}(M_0^0 - M_0^\infty) \\[2mm]
M_1^0 = \dfrac{32}{45}\dfrac{\eta_M^s\eta_M^d}{(\eta_M^s+\eta_M^d)^2}\dfrac{(7\eta_M^{s\,2}+10\eta_M^s\eta_M^d+4\eta_M^{d\,2})}{(2\eta_M^s+\eta_M^d)^2}\left[\dfrac{\eta_M^s}{3}\left(\dfrac{1}{k_M^e}+\dfrac{1}{k_K^e}\right)-\dfrac{\eta_M^d}{2}\left(\dfrac{1}{\mu_M^e}+\dfrac{1}{\mu_K^e}\right)\right] \\[2mm]
M_{-1}^\infty = \dfrac{16}{15}\dfrac{k_M^e\mu_M^e}{(3k_M^e+\mu_M^e)^2}\dfrac{(63k_M^{e\,2}+60\mu_M^e k_M^e+16\mu_M^{e\,2})}{(3k_M^e+2\mu_M^e)^2}\cdot\left[3k_M^e\left(\dfrac{1}{\eta_M^s}+\dfrac{1}{\eta_K^s}\right)-2\mu_M^e\left(\dfrac{1}{\eta_M^d}+\dfrac{1}{\eta_K^d}\right)\right]
\end{cases}
\tag{11}
$$

Using (6), the Burger model gives:

$$
\begin{cases}
\tilde{E}_{Bu\_3}^{-1} = \dfrac{1}{9k_M^e(d_c)} + \dfrac{1}{3\mu_M^e(d_c)} + \left(\dfrac{1}{3\eta_M^s(d_c)} + \dfrac{2}{3\eta_M^d(d_c)}\right)t + \dfrac{1}{9k_K^e(d_c)}\left(1-e^{-t/\tau_K^s(d_c)}\right) + \dfrac{1}{3\mu_K^e(d_c)}\left(1-e^{-t/\tau_K^d(d_c)}\right) \\[3mm]
\tilde{\mu}_{Bu\_23} = \dfrac{\mu_K^e(d_c)\mu_M^e(d_c)\eta_M^d(d_c)}{\left(1-e^{-t/\tau_K^d(d_c)}\right)\mu_M^e(d_c)\eta_M^d(d_c) + \mu_K^e(d_c)\left(\eta_M^d(d_c)+2.t.\mu_M^e(d_c)\right)}
\end{cases}
\tag{12}
$$

where $\quad \tau_K^s(d_c) = \dfrac{\eta_K^s(d_c)}{3k_K^e(d_c)}, \qquad \tau_K^d(d_c) = \dfrac{\eta_K^d(d_c)}{2\mu_K^e(d_c)}$

2.1.2 MM model
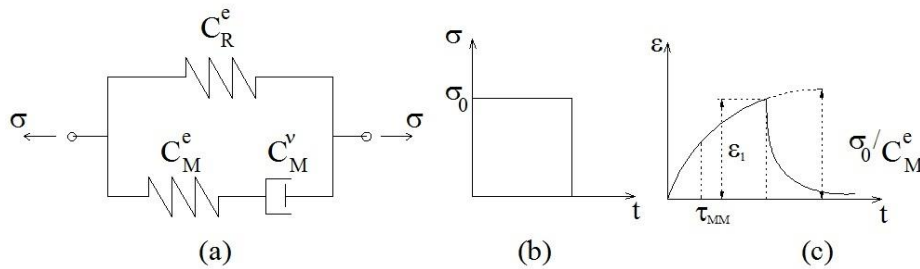
Figure 3. MM model (a) and its deformation response (c) under the effect of a constant stress (b).

In the MM model, two moduli in (7) are:

$$
\tilde{k}_{MM}^*(p,d_c) = k_R^e(d_c) + \left[\dfrac{1}{k_M^e(d_c)} + \dfrac{1}{p\eta_M^s(d_c)/3}\right]^{-1}; \quad \tilde{\mu}_{MM}^*(p,d_c) = \mu_R^e(d_c) + \left[\dfrac{1}{\mu_M^e(d_c)} + \dfrac{1}{p\eta_M^d(d_c)/2}\right]^{-1}
\tag{13}
$$

in which there are 6 parameters:

$$\begin{cases} \dfrac{1}{k_R^e(d_c)} = \dfrac{1+Q_M^v d_c}{k_R^e}, \quad \dfrac{1}{k_M^e(d_c)} = \dfrac{1+Q_M^e d_c}{k_R^e + k_M^e - \dfrac{k_R^e(1+Q_M^e d_c)}{1+Q_M^v d_c}}, \quad \dfrac{1}{\eta_M^s(d_c)} = \dfrac{(1+Q_M^v d_c)^2}{\eta_M^s(1+Q_M^v d_c)-3d_c k_R^e Q_1^0}; \\[4mm] \dfrac{1}{\mu_R^e(d_c)} = \dfrac{1+M_M^v d_c}{\mu_R^e}, \quad \dfrac{1}{\mu_M^e(d_c)} = \dfrac{1+M_M^e d_c}{\mu_R^e + \mu_M^e - \dfrac{\mu_R^e(1+M_M^e d_c)}{1+M_M^v d_c}}, \quad \dfrac{1}{\eta_M^d(d_c)} = \dfrac{(1+M_M^v d_c)^2}{\eta_M^d(1+M_M^v d_c)-2d_c \mu_R^e M_1^0} \end{cases} \quad (14)$$

where

$$\begin{cases} Q_M^v = Q_0^0 = \dfrac{4}{3}\dfrac{k_R^e(3k_R^e + 4\mu_R^e)}{\mu_R^e(3k_R^e + \mu_R^e)}; \; Q_1^0 = \dfrac{2}{9}\dfrac{(9k_R^{e2}+6k_R^e\mu_R^e+4\mu_R^{e2})(-3k_R^e\eta_M^d+2\mu_R^e\eta_M^s)}{\mu_R^{e2}(3k_R^e+\mu_R^e)^2}; \\[4mm] Q_M^e = Q_0^\infty = \dfrac{4}{3}\dfrac{(k_R^e+k_M^e)[3(k_R^e+k_M^e)+4(\mu_R^e+\mu_M^e)]}{(\mu_R^e+\mu_M^e)[3(k_R^e+k_M^e)+(\mu_R^e+\mu_M^e)]}; \\[4mm] M_M^e = M_0^\infty = \dfrac{16}{45}\left(\dfrac{3(k_R^e+k_M^e)+4(\mu_R^e+\mu_M^e)}{3(k_R^e+k_M^e)+(\mu_R^e+\mu_M^e)}\right)\left(\dfrac{9(k_R^e+k_M^e)+4(\mu_R^e+\mu_M^e)}{3(k_R^e+k_M^e)+2(\mu_R^e+\mu_M^e)}\right) \\[4mm] M_M^v = M_0^0 = \dfrac{16}{45}\dfrac{(3k_R^e+4\mu_R^e)(9k_R^e+4\mu_R^e)}{9k_R^{e2}+9k_R^e\mu_R^e+2\mu_R^{e2}}, \; M_1^0 = \dfrac{8}{45}\dfrac{(63k_R^{e2}+60k_R^e\mu_R^e+16\mu_R^{e2})(3k_R^e\eta_M^d-2\mu_R^e\eta_M^s)}{(9k_R^{e2}+9k_R^e\mu_R^e+2\mu_R^{e2})} \end{cases} \quad (15)$$

Using (6) for the case of isotropic distribution of cracks, MM model gives:

$$\begin{cases} \tilde{E}_{MM\_3}^{-1} = \dfrac{1}{9[k_R^e(d_c)+k_M^e(d_c)]} + \dfrac{1}{3[\mu_R^e(d_c)+\mu_M^e(d_c)]} + \dfrac{k_M^e(d_c)(1-e^{-t/\tau_{MM}^s(d_c)})}{9k_R^e(d_c)\left(k_R^e(d_c)+k_M^e(d_c)\right)} + \dfrac{\mu_M^e(d_c)(1-e^{-t/\tau_{MM}^d(d_c)})}{3\mu_R^e(d_c)\left(\mu_R^e(d_c)+\mu_M^e(d_c)\right)}; \\[4mm] \tilde{\mu}_{MM\_23} = \dfrac{\mu_R^e(d_c)\left(\mu_R^e(d_c)+\mu_M^e(d_c)\right)}{\left(1-e^{-t/\tau_{MM}^d(d_c)}\right)\mu_M^e(d_c)+\mu_R^e(d_c)} \end{cases} \quad (16)$$

with $$\tau_{MM}^s(d_c) = \dfrac{\eta_M^s(d_c)\left(k_R^e(d_c)+k_M^e(d_c)\right)}{3k_R^e(d_c)k_M^e(d_c)}, \quad \tau_{MM}^d(d_c) = \dfrac{\eta_M^d(d_c)\left(\mu_R^e(d_c)+\mu_M^e(d_c)\right)}{2\mu_R^e(d_c)\mu_M^e(d_c)} \quad (17)$$

2.2. Parallel distribution of cracks

The apparent compliance tensor s^* of the micro-cracked medium is transversely isotropic and is written in the Walpole base in the form:

$$S^* = \sum_{i=1}^{6} \tilde{s}_i^* E_i \quad (18)$$

To determine the parameters $\tilde{s}_i^*$, we consider different types of loadings. Nguyen [29] expressed the apparent macroscopic law in the Walpole base based on the moving solution of the problem of brittle fracture. For example, the case of uniaxial tension $\Sigma = \Sigma N$ in the direction of the normal displacement jump to the crack plane (mode I) gives us $\tilde{s}_2^*$ and $\tilde{s}_5^*$.

$$\bar{\varepsilon}^* = \left[\left(s_2^* + \dfrac{8(1-\nu^*)d_c}{3\mu^*}\right)N + s_5^* T\right]\Sigma^* = \left[\tilde{s}_2^* N + \tilde{s}_5^* T\right]\Sigma^* \quad (19)$$

with $N = \mathbf{n} \otimes \mathbf{n}$; $T = 1 - N$; $\tilde{s}_2^* = s_2^*(1+N^* d_c)$ where $N^* = \dfrac{16(1-\nu^{*2})d_c}{3}$ and $\tilde{s}_5^* = s_5^*$

For the sake of completeness, the Walpole base formulas available in the literature are recalled in the [29]. For the other cases of loadings, transverse traction and transverse shear, see [30].

2.2.1 Burger model

In Burger model, $\tilde{s}_2^*$ is written as:

$$\tilde{s}_2^* = s_{M2}^e(d_c) + \frac{s_{M2}^v(d_c)}{p} + \left(\frac{1}{s_{K2}^e(d_c)} + \frac{p}{s_{K2}^v(d_c)} \right)^{-1} \qquad (20)$$

with

$$s_{M2}^e(d_c) = s_{M2}^e(1+N_M^e d_c), \; s_{M2}^v(d_c) = s_{M2}^v(1+N_M^v d_c), \; s_{K2}^e(d_c) = s_{K2}^e(1+N_K^e d_c), \; s_{K2}^v(d_c) = s_{K2}^v(1+N_K^v d_c) \qquad (21)$$

where

$$N_M^e = N_0^\infty, \quad N_K^e = N_0^0 + N_1^0 \frac{s_{M2}^v}{s_{K2}^e} + (N_0^0 - N_0^\infty)\frac{s_{M2}^e}{s_{K2}^e}; N_M^v = N_0^0, \quad N_K^v = N_0^\infty + N_{-1}^0 \frac{s_{M2}^e}{s_{K2}^v} + (N_0^\infty - N_0^0)\frac{s_{M2}^v}{s_{K2}^v} \qquad (22)$$

and

$$
\left\{
\begin{aligned}
&s_{M2}^e = \frac{1}{2\mu_M^e(1+\nu_M)}, \quad s_{K2}^e = \frac{1}{2\mu_K^e(1+\nu_K)}, \; s_{M2}^v = \frac{1}{\eta_M^d(1+\nu_{vM})}, \quad s_{K2}^v = \frac{1}{\eta_K^d(1+\nu_{vK})}; \\
&s_{K1}^e(d_c) = s_{K1}^e = \frac{1-\nu_K}{2\mu_K^e(1+\nu_K)}, \; s_{K1}^v(d_c) = s_{K1}^v = \frac{1-\nu_{vK}}{\eta_K^d(1+\nu_{vK})}; \\
&s_{M1}^e(d_c) = s_{M1}^e = \frac{1-\nu_M}{2\mu_M^e(1+\nu_M)}, \; s_{M1}^v(d_c) = s_{M1}^v = \frac{1-\nu_{vM}}{\eta_M^d(1+\nu_{vM})} \\
&s_{K3}^e(d_c) = s_{K3}^e = \frac{1}{2\mu_K^e}, \; s_{K3}^v(d_c) = s_{K3}^v = \frac{1}{\eta_K^d}; \\
&s_{M3}^e(d_c) = s_{M3}^e = \frac{1}{2\mu_M^e}, \; s_{M3}^v(d_c) = s_{M3}^v = \frac{1}{\eta_M^d}; \; s_{K4}^e(d_c) = s_{K4}^e\left(1+P_K^e d_c\right), \\
&s_{K4}^v(d_c) = s_{K4}^v\left(1+P_K^v d_c\right); \; s_{M4}^e(d_c) = s_{M4}^e\left(1+P_M^e d_c\right), \; s_{M4}^v(d_c) = s_{M4}^v\left(1+P_M^v d_c\right); \\
&s_{K5}^e(d_c) = s_{K5}^e = -\frac{\nu_K}{2\mu_K^e(1+\nu_K)}, \; s_{K5}^v(d_c) = s_{K5}^v = -\frac{\nu_{vK}}{\eta_K^d(1+\nu_{vK})}; \\
&s_{M5}^e(d_c) = s_{M5}^e = -\frac{\nu_M}{2\mu_M^e(1+\nu_M)}, \; s_{M5}^v(d_c) = s_{M5}^v = -\frac{\nu_{vM}}{\eta_M^d(1+\nu_{vM})}
\end{aligned}
\right. \qquad (23)
$$

with

$$
\left\{
\begin{aligned}
&P_K^e = P_0^0 + P_1^0\, s_{M4}^v/s_{K4}^e + (P_0^0 - P_0^\infty)s_{M4}^e/s_{K4}^e; \; P_M^e = P_0^\infty; \; P_M^v = P_0^0; \\
&P_K^v = P_0^\infty + P_{-1}^\infty s_{M4}^e/s_{K4}^v + (P_0^\infty - P_0^0)s_{M4}^v/s_{K4}^v; \; \nu_{vM} = \frac{\eta_M^s - \eta_M^d}{2\eta_M^s + \eta_M^d}; \\
&P_0^0 = \frac{16\left(\eta_M^s + 2\eta_M^d\right)}{9\left(\eta_M^s + \eta_M^d\right)}; \; P_1^0 = \frac{16\eta_M^s \eta_M^d}{9\left(\eta_M^s + \eta_M^d\right)}\left[\eta_M^s\left(\frac{1}{3k_M} + \frac{1}{3k_K}\right) - \eta_M^d\left(\frac{1}{2\mu_M} + \frac{1}{2\mu_K}\right)\right]; \\
&P_0^\infty = \frac{16\left(3k_M + 4\mu_M\right)}{9\left(3k_M + 2\mu_M\right)}; \; P_{-1}^\infty = \frac{\frac{32k_M\mu_M}{3\left(3k_M + 2\mu_M\right)^2}\left[3k_M\left(\frac{1}{\eta_M^s} + \frac{1}{\eta_K^s}\right) - 2\mu_M\left(\frac{1}{\eta_M^d} + \frac{1}{\eta_K^d}\right)\right]}{9\left(3k_M + 2\mu_M\right)}
\end{aligned}
\right. \qquad (24)
$$

It is worth noting that only $\tilde{s}_2^*$, $\tilde{s}_4^*$ depend on the density of cracks d_c.

Using (6) for the case of transversely isotropic distribution of cracks, Burger model gives:

$$\tilde{E}_{Bu\_3}^{-1} = \frac{s_1(t)}{-2s_5^2(t) + s_1(t)s_2(t)}; \; \tilde{\mu}_{Bu\_23} = \frac{2}{s_4(t)} \qquad (25)$$

$$\text{with} \begin{cases} s_1(t) = s_{M1}^e(d_c) + s_{M1}^v(d_c).t + s_{K1}^e(d_c)\ (1 - e^{-t/\tau_{K1}(d_c)}) \text{ with } \tau_{K1}(d_c) = s_{K1}^e(d_c)/s_{K1}^v(d_c); \\ s_2(t) = s_{M2}^e(d_c) + s_{M2}^v(d_c).t + s_{K2}^e(d_c)\ (1 - e^{-t/\tau_{K2}(d_c)}) \text{ with } \tau_{K2}(d_c) = s_{K2}^e(d_c)/s_{K2}^v(d_c); \\ s_4(t) = s_{M4}^e(d_c) + s_{M4}^v(d_c).t + s_{K4}^e(d_c)\ (1 - e^{-t/\tau_{K4}(d_c)}) \text{ with } \tau_{K4}(d_c) = s_{K4}^e(d_c)/s_{K4}^v(d_c); \\ s_5(t) = s_{M5}^e + s_{M5}^v * t + s_{K5}^e\ (1 - e^{-t/\tau_{K5}}) \text{ with } \tau_{K5} = s_{K5}^e/s_{K5}^v \end{cases} \tag{26}$$

2.2.2 MM model

The same procedure is adopted for the case of the MM model to derive the effective medium. If the homogenized medium has the sample rheological behavior (i.e., MM), it should satisfy the following condition:

$$C_{MM\_d_c}^* = C_R^e(d_c) + \left[S_M^e(d_c) + \frac{1}{p} S_M^v(d_c) \right]^{-1} \tag{27}$$

The best approximation of the apparent rigidity $\square_{MM\_d_c}^*$ in short and long terms gives:

$$\tilde{c}_2^{*-1} = c_{R2}^e(d_c) + [1/c_{M2}^e(d_c) + \frac{1}{p}(1/c_{M2}^v(d_c))]^{-1} \tag{28}$$

in which

$$c_{R2}^e(d_c) = \frac{c_{R2}^e}{(1+N_0^0 d_c)}, c_{M2}^e(d_c) = \frac{(c_{R2}^e + c_{M2}^e)}{(1+N_0^\infty d_c)} - c_{R2}^e(d_c); c_{M2}^v(d_c) = \frac{c_{M2}^v}{(1+N_0^0 d_c)} \left(1 - \frac{N_1^0 d_c}{1+N_0^0 d_c} \frac{c_{R2}^e}{c_{M2}^v}\right) \tag{29}$$

$$\text{with } N_0^0 = \frac{12k_R^e(3k_R^e + 4\mu_R^e)}{(3k_R^e + \mu_R^e)^2},\ N_1^0 = \frac{4(3k_R^e - 2\mu_R^e)(3k_R^e\eta_M^d - 2\mu_R^e\eta_M^s)}{(3k_R^e + \mu_R^e)^3}, N_0^\infty = \frac{12(k_R^e + k_M^e)\left[(3(k_R^e + k_M^e) + 4(\mu_R^e + \mu_M^e))\right]}{\left[3k_R^e + k_M^e) + (\mu_R^e + \mu_M^e)\right]^2} \tag{30}$$

And for other parameters, the MM model gives:

$$\begin{cases} c_{R1}^e(d_c) = c_{R1}^e = \frac{2\mu_R^e(1+\nu_R)}{1-\nu_R}, & c_{M1}^e(d_c) = c_{M1}^e = \frac{2\mu_M^e(1+\nu_M)}{1-\nu_M}, c_{M1}^v(d_c) = c_{M1}^v = \frac{\eta_M^d(1+\nu_{vM})}{1-\nu_{vM}} \\ c_{R3}^e(d_c) = c_{R3}^e = 2\mu_R^e, & c_{M3}^e(d_c) = c_{M3}^e = 2\mu_M^e, c_{M3}^v(d_c) = c_{M3}^v = \eta_M^d; \\ c_{R4}^e(d_c) = \frac{c_{K4}^e}{(1+P_0^0 d_c)}, & c_{M4}^e(d_c) = \frac{(c_{R4}^e + c_{M4}^e)}{(1+P_0^\infty d_c)} - c_{R4}^e(d_c), c_{M4}^v(d_c) = \frac{c_{M4}^v(1+P_0^0 d_c) - c_{R4}^e P_1^0 d_c}{(1+P_0^0 d_c)^2}; \\ c_{R5}^e(d_c) = c_{R5}^e = -\frac{2\mu_R^e(1+\nu_R)}{\nu_R}, & c_{M5}^e(d_c) = c_{M5}^e = -\frac{2\mu_M^e(1+\nu_M)}{\nu_M}, c_{M5}^v(d_c) = c_{M5}^v = -\frac{\eta_M^d(1+\nu_{vM})}{\nu_{vM}} \end{cases} \tag{31}$$

$$\text{with } \nu_{vM} = \frac{\eta_M^s - \eta_M^d}{2\eta_M^s + \eta_M^d};\ P_0^0 = \frac{48k_R^e + 64\mu_R^e}{27k_R^e + 18\mu_R^e};\ P_1^0 = \frac{16(3k_R^e\eta_M^d - 2\mu_R^e\eta_M^s)}{9(3k_R^e + 2\mu_R^e)^2}; P_0^\infty = \frac{16\left[3(k_R^e + k_R^e) + 4(\mu_R^e + \mu_M^e)\right]}{9\left[3(k_R^e + k_R^e) + 2(\mu_R^e + \mu_M^e)\right]} \tag{32}$$

The MM model gives the effective Young and shear moduli:

$$\tilde{E}_{Bu\_3}^{-1} = c_2(t);\ \tilde{\mu}_{Bu\_23} = \frac{c_4(t)}{2} \tag{33}$$

$$\text{where } \begin{cases} c_2(t) = c_{R2}^e(d_c) + c_{M2}^e(d_c).e^{-t/\tau_{M2}(d_c)} \text{ with } \tau_{M2}(d_c) = c_{M2}^v(d_c)/c_{M2}^e(d_c); \\ c_4(t) = c_{R4}^e(d_c) + c_{M4}^e(d_c).e^{-t/\tau_{M4}(d_c)} \text{ with } \tau_{M4}(d_c) = c_{M4}^v(d_c)/c_{M4}^e(d_c) \end{cases} \tag{34}$$

3. THE INTERFACIAL LAWS

The interface law links the stress vector to the jump of the displacement across the crack via a diagonal matrix. Since the joint is soft and has a very small thickness, it can be replaced

by an interface law defined along the limit surface. Its mechanical behavior can therefore be obtained by asymptotic techniques where the thickness of the joint tends to zero. Having the interface law, the hybrid structure problem can be solved by the finite element method. Therefore, the terms C_N and C_T that correspond to the normal and tangential jumps of the displacement, are given by (for more details, see [18]):

$$C_N = \lim_{e \to 0} \frac{\tilde{C}_{3333}}{e}, \quad C_T = \lim_{e \to 0} \frac{\tilde{C}_{1313}}{e} \tag{35}$$

in which e is the thickness of the micro-cracked EM material.

Noting that S the area of the surface, $d_c = \dfrac{N_c a^3}{S} = N a^3$ with the number of cracks per unit of area in the case of 2D structure.

A combination of (6), (12), (16), (25), (33), and (35) yields the expressions for the interface stiffnesses C_N, C_T of Burger and MM models for two considered cases.

Case of isotropic cracks:

$$\begin{cases} C_{Bu\_N}^{iso} = \dfrac{9}{d_c\left[\left(1-e^{-\frac{3k_K^e Q_K^v}{\eta_K^s Q_K^e}t}\right)\dfrac{Q_K^e}{k_K^e}+\dfrac{Q_M^e}{k_M^e}+3\left(\left(1-e^{-\frac{2\mu_K^e M_K^v}{\eta_K^d M_K^e}t}\right)\dfrac{M_K^e}{\mu_K^e}+\dfrac{M_M^e}{\mu_M^e}+t.\left(\dfrac{2M_M^v}{\eta_M^d}+\dfrac{Q_M^v}{\eta s}\right)\right)\right]}; \\[2em] C_{Bu\_T}^{iso} = \dfrac{1}{d_c\left[\left(1-e^{-\frac{3k_K^e Q_K^v}{\eta_K^s Q_K^e}t}\right)\dfrac{M_K^e}{\mu_K^e}+\dfrac{M_M^e}{\mu_M^e}+2.t.\dfrac{M_M^v}{\eta_M^d}\right]} \end{cases} \tag{36}$$

$$\begin{cases} C_{MM\_N}^{iso} = \dfrac{9}{d_c\left[\left(1-e^{-At}\right)\dfrac{Q_M^v}{k_R^e}+\dfrac{Q_M^e}{k_R^e+k_M^e}e^{-At}+3\left(\left(1-e^{-Bt}\right)\dfrac{M_M^v}{\mu_R^e}+\dfrac{M_M^e}{\mu_R^e+\mu_M^e}e^{-Bt}\right)\right]}; \\[2em] C_{MM\_T}^{iso} = \dfrac{1}{d_c\left[\left(1-e^{-Bt}\right)M_M^v\left(\mu_R^e+\mu_M^e\right)+\mu_R^e M_M^e e^{-Bt}\right]} \end{cases} \tag{37}$$

with
$$A = \dfrac{3k_R^e\left[k_R^e\left(Q_M^e-Q_M^v\right)-k_M^e Q_M^v\right]}{\left(k_R^e+k_M^e\right)\left(3Q_1^0 k_R^e-Q_M^v \eta_M^s\right)}; \quad B = \dfrac{2\mu_R^e\left[\mu_R^e\left(M_M^e-M_M^v\right)-\mu_M^e M_M^v\right]}{\left(\mu_R^e+\mu_M^e\right)\left(2M_1^0 \mu_R^e-M_M^v \eta_M^d\right)} \tag{38}$$

Case of transversely isotropic cracks:

$$C_{Bu\_N}^{//} = \dfrac{1}{d_c\left[\left(1-e^{-\frac{s_{K2}^v N_K^v}{s_{K2}^e N_K^e}t}\right)N_K^e s_{K2}^e+N_M^e s_{M2}^e+N_M^v s_{M2}^v.t\right]}; \quad C_{Bu\_T}^{//} = \dfrac{2}{d_c\left[\left(1-e^{-\frac{s_{K4}^v P_K^v}{s_{K4}^e P_K^e}t}\right)P_K^e s_{K4}^e+P_M^e s_{M4}^e+P_M^v s_{M4}^v.t\right]} \tag{39}$$

$$C_{MM\_N}^{//} = \dfrac{1}{d_c}\left[e^{-Ct}\dfrac{\left(c_{R2}^e+c_{M2}^e\right)}{N_0^\infty}+\left(1-e^{-Ct}\right)\dfrac{c_{R2}^e}{N_0^0}\right]; \quad C_{MM\_T}^{//} = \dfrac{1}{2d_c}\left[e^{-Dt}\dfrac{\left(c_{R4}^e+c_{M4}^e\right)}{P_0^\infty}+\left(1-e^{-Dt}\right)\dfrac{c_{R4}^e}{P_0^0}\right] \tag{40}$$

with
$$C = \dfrac{N_0^0\left[\left(c_{R2}^e+c_{M2}^e\right)N_0^0-c_{R2}^e N_0^\infty\right]}{\left(c_{M2}^v N_0^0-c_{R2}^e N_1^0\right)N_0^\infty}; \quad D = \dfrac{P_0^0\left[\left(c_{R4}^e+c_{M4}^e\right)P_0^0-c_{R4}^e P_0^\infty\right]}{\left(c_{M4}^v P_0^0-c_{R4}^e P_1^0\right)P_0^\infty} \tag{41}$$

4. DISCUSSION OF THE PROPOSED NONLINEAR INTERFACIAL LAW

The expressions (36) - (41) show that C_N, C_T depend not only on the time, but also on the crack density d_c. In order to discuss the evolution of the interface properties, the concrete described by Burger model and the hybrid mortar represented by MM model are considered in this section. The properties of these two materials are given in Table 1 [30].

Table 1. The effective properties of hybrid mortar with $d_c = 0.0$

Model	$k_M^e(d_c)$ (MPa)	$\mu_M^e(d_c)$ (MPa)	$\eta_M^s(d_c)$ (MPa.s)	$\eta_M^d(d_c)$ (MPa.s)	$k_K^e(d_c)$ (MPa)	$\mu_K^e(d_c)$ (MPa)	$\eta_K^s(d_c)$ (MPa.s)	$\eta_K^d(d_c)$ (MPa.s)	$k_R^e(d_c)$ (MPa)	$\mu_R^e(d_c)$ (MPa)
Burger	2404	1655	3.35 10^8	1.54 10^8	1257	866	3.43 10^6	1.57 10^8	-	-
MM	2404	1655	3.35 10^8	1.54 10^8	-	-	-	-	1257	866

Figures 4-7 present the dependence of the normal and tangential stiffnesses of the interface on time. The MM model shows a dramatically decrease followed by a constant asymptote. The stiffnesses predicted by the MM model reach the asymptotic limit after t ~ 5 days for the isotropic distribution of cracks and t ~ 2.5 days for the parallel distribution of cracks. The Burger model exhibits a rapid decrease during ~2.5 days followed by a progressive decrease of the stiffnesses.
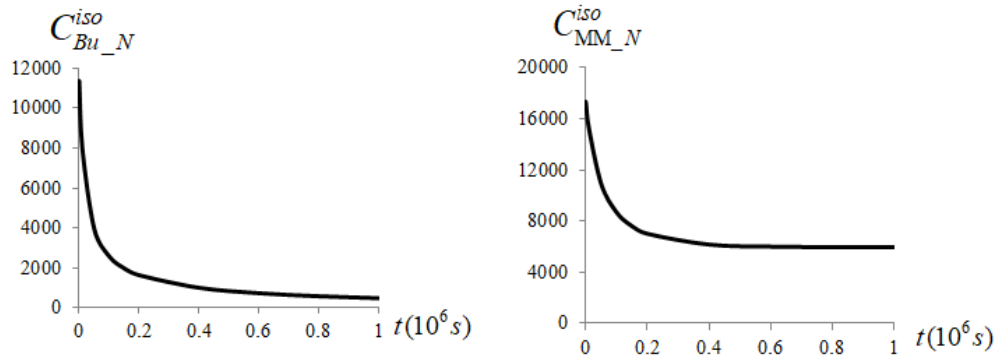
Figure 4. The normal stiffnesses of the interface for Burger and MM models, case of isotropy crack distribution $(d_c = 0.1)$.
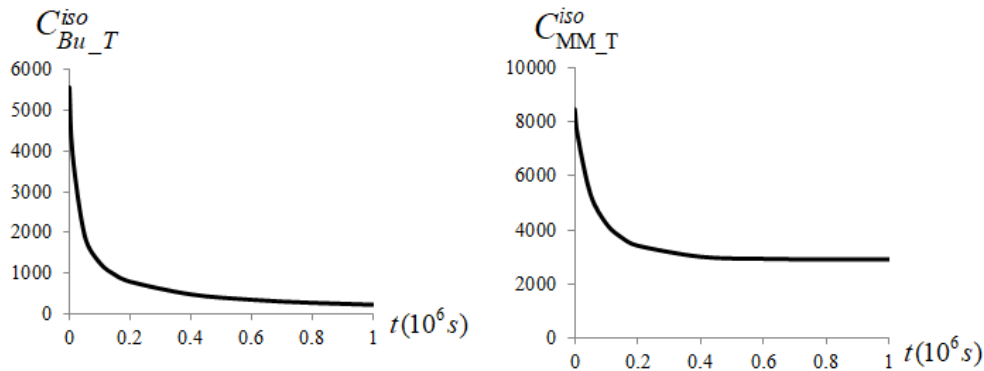
Figure 5. The tangential stiffnesses of the interface for Burger and MM models, case of isotropy crack distribution $(d_c = 0.1)$.
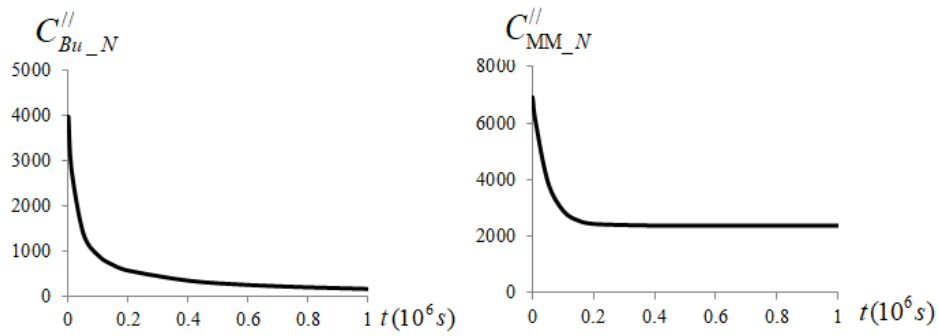
Figure 6. The normal stiffnesses of the interface for Burger and MM models, case of transversely isotropy crack distribution $(d_c = 0.1)$.
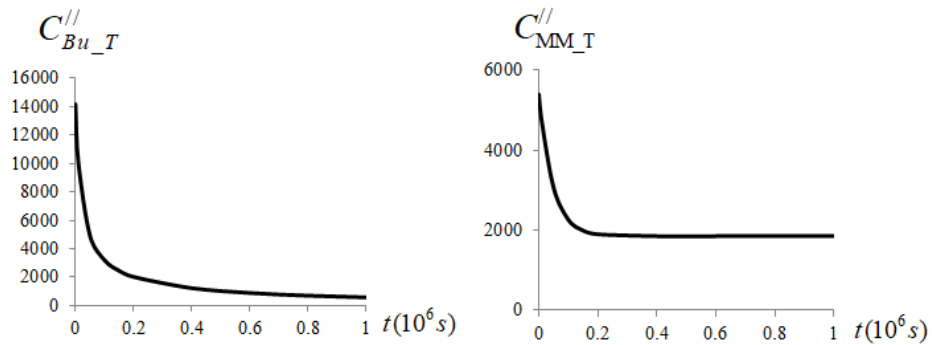
Figure 7. The tangential stiffnesses of the interface for Burger and MM models, case of of transversely isotropy crack distribution $(d_c = 0.1)$.

As a function of crack density, both Burger and the MM models depend strongly on d_c and tend rapidly to zero when d_c increases (see Figs. 8-11). In almost all cases (except $C_T^{//}$ at $t = 0s$ case of transversely isotropy crack distribution), the MM model gives the values of C_N, C_T higher than that of the Burger model. When the crack density is high $(d_c > 0.15)$, both C_N, C_T are very low and no distinct difference between the Burger and MM models can be seen. Comparing Fig. 8 with Fig. 6, and Fig. 9 with Fig. 7 one can see that C_N, C_T in the case of transversely isotropic cracks are lower than the ones in case of isotropic cracks.
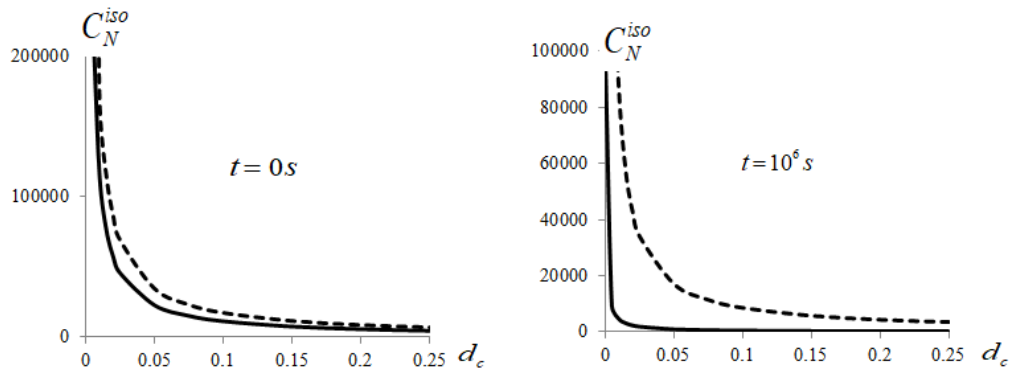
Figure 8. Evolution of the normal stiffnesses of the interface as a function of crack density d_c for Burger model (continuous line) and MM model (dash-line), case of isotropy crack distribution.
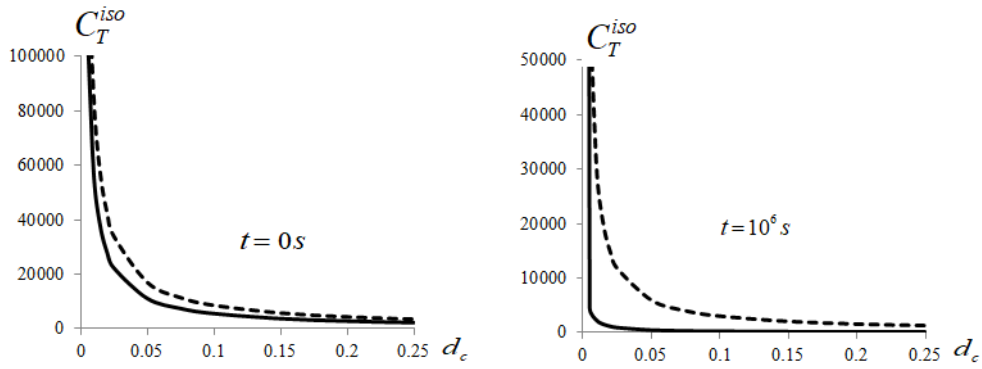
Figure 9. Evolution of the tangential stiffnesses of the interface as a function of crack density d_c for Burger model (continuous line) and MM model (dash-line), case of isotropy crack distribution.
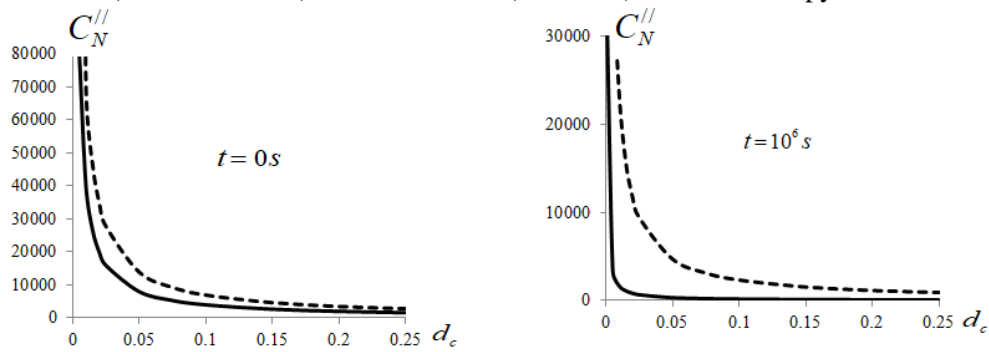
Figure 10. Evolution of the normal stiffnesses of the interface as a function of crack density d_c for Burger model (continuous line) and MM model (dash-line), case of transversely isotropy crack distribution.
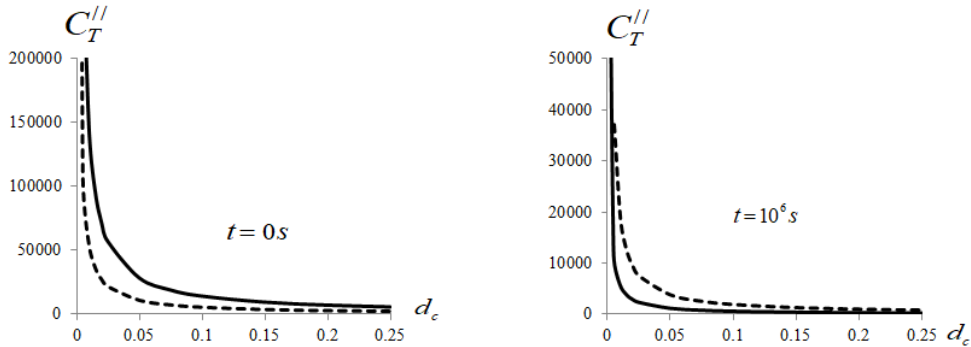
Figure 11. Evolution of the tangential stiffnesses of the interface as a function of crack density d_c for Burger model (continuous line) and MM model (dash-line), case of transversely isotropy crack distribution.

5. CONCLUSIONS

This study describes the procedure to identify the viscoelastic interfacial laws for hybrid structures. In such a structure, the more solid material is assumed to be undamaged and elastic, while the weaker material is viscoelastic. The interface between them behaves similarly to the weaker material Analytical expressions describing the interfacial laws are derived by using two rheological models: Burger and Modified Maxell. The applications of these two models for the case of hydric mortar are discussed. It is shown that the normal and

tangential stiffnesses of the interface depend not only on the time but also strongly on the crack density. The MM model leads to a finite asymptotic limit for the values of $C_N(t), C_T(t)$ while these coefficients vanish after several days with Burger's predictions. Besides, there is no distinct difference between Burger and MM models in the case of assuming the same high crack density in the interface (i.e., $d_c \geq 0.15$), and the values of C_N, C_T are very low. The advantage of non-linear interfacial law characterized by C_N, C_T consists in the independence of the number of elements used in the interface. Therefore, this is a good solution to model the effective viscoelastic behavior of the hybrid structure thanks to a low numerical cost. The established formulations from this study for the normal and tangential stiffnesses can be applied to the analysis of multi-layered systems exhibiting either elastic or viscoelastic behavior. In a future study, the relevance of the proposed method needs to be evaluated by comparing the numerical results with the test data.

REFERENCES

[1]. E. Munch, M. E. Launey, D. H. Alsem, E. Saiz, A. P. Tomsia, R. O. Ritchie, Tough, bio-inspired hybrid materials, Science, 322 (2008) 1516-1520.

[2]. J. Zhang, K. Chaisombat, S. He, C. H. Wang, Hybrid composite laminates reinforced with glass/carbon woven fabrics for lightweight load bearing structures, Mater Design, 36 (2012) 75-80. https://doi.org/10.1016/j.matdes.2011.11.006

[3]. T. T. N. Nguyen, N. H. Tran, Modelling of contact interface between two material layers in hybrid structures. Transport and Communications Science Journal, 71 (2020) 419-430. https://doi.org/10.25073/tcsj.71.4.10

[4]. P. A. Teeuwen, C. S. Kleinman, H. H. Snijder, H. Hofmeyer, Experiments and FE-model for a connection between steel frames and precast concrete infill panels (Stuttgart), 2nd International Symposium on Connections between Steel and Concrete, 2007 Sep 04-07, Ibidem-Verlag (2007), 1093-1102.

[5]. H. Tan, Y. Huang, C. Liu, P. H. Geubelle, The Mori–Tanaka method for composite materials with nonlinear interface debonding, Int J Plasticity, 21 (2005) 1890-1918. https://doi.org/10.1016/j.ijplas.2004.10.001

[6]. J. W. Giancapro, C. G. Papakonstantinou, P. N. Balagura. Flexural response of inorganic hybrid composites with E-glass and carbon fibers, J Eng Mater Technol, 132 (2010) 1–8. https://doi.org/10.1115/1.4000670

[7]. Z. I. Djamai, M. Bahrar, F. Salvatore, A.S. Larbi, M. El Mankibi, Textile reinforced concrete multiscale mechanical modelling: Application to TRC sandwich panels, Finite Elem Anal Des, 135 (2017) 22-35. https://doi.org/10.1016/j.finel.2017.07.003

[8]. M. Dhanasekar, A.W. Page, P.W. Kleeman, The failure of brick masonry under biaxial stresses, Proceedings of the Institution of Civil Engineers, 79 (1985) 295–313. https://doi.org/10.1680/iicep.1985.992

[9]. L. H. Sneed, T. D'Antino, C. Carloni, Investigation of bond behavior of PBO fiber-reinforced cementitious matrix composite-concrete interface, ACI Mater J, 111 (2014) 569-580.

[10]. O. Awani, T. El-Maaddawy, N. Ismail, Fabric-reinforced cementitious matrix: A promising strengthening technique for concrete structures, Constr Build Mater, 132 (2017) 94-111. https://doi.org/10.1016/j.conbuildmat.2016.11.125

[11]. F. de Andrade Silva, M. Butler, S. Hempel, R. D. Toledo Filho, V. Mechtcherine, Effects of elevated temperatures on the interface properties of carbon textile-reinforced concrete, Cement Concrete Comp, 48 (2014) 26-34. https://doi.org/10.1016/j.cemconcomp.2014.01.007

[12]. H. R. Lotfi, P.B. Shing, Interface model applied to fracture of masonry structures, J Struct Eng, 120 (1994) 63-80. https://doi.org/10.1061/(ASCE)0733-9445(1994)120:1(63)

[13]. M. R. Wisnom, Modelling the effect of cracks on interlaminar shear strength, Compos Part A-Appl S, 27 (1996) 17–24. https://doi.org/10.1016/1359-835X(95)00007-O

[14]. L. Ombres, Debonding analysis of reinforced concrete beams strengthened with fibre reinforced cementitious mortar, Eng Fract Mech, 81 (2012) 94-109. https://doi.org/10.1016/j.engfracmech.2011.06.012

[15]. S. M. Raoof, L. N. Koutas, D. A. Bournas, Bond between textile-reinforced mortar (TRM) and concrete substrates: experimental investigation, Compo Part B-Eng, 98 (2016) 350-361. https://doi.org/10.1016/j.compositesb.2016.05.041

[16]. I. Carol, C. M. Lopez, O. Roa, Micromechanical analysis of quasi-brittle materials using fracture-based interface elements, Int J Numer Meth Eng, 52 (2001) 193-215. https://doi.org/10.1002/nme.277

[17]. M. R. Wisnom, Modelling discrete failures in composites with interface elements, Compos Part A-Appl S, 41 (2010) 795-805. https://doi.org/10.1016/j.compositesa.2010.02.011

[18]. A. Rekik, F. Lebon, Homogenization methods for interface modeling in damaged masonry. Adv Eng Softw, 46 (2012) 35-42. https://doi.org/10.1016/j.advengsoft.2010.09.009

[19]. A. Needleman, D. Coker, A. J. Rosakis, Fast crack growth along interfaces, Lat Am J Solids Stru, 2 (2005) 5-15.

[20]. N. Ranganathan, K. Oksman, S. K. Nayak, M. Sain, Structure property relation of hybrid biocomposites based on jute, viscose and polypropylene: The effect of the fibre content and the length on the fracture toughness and the fatigue properties, Compos Part A-Appl S, 83 (2016) 169-175. https://doi.org/10.1016/j.compositesa.2015.10.037

[21]. J. Reinoso, M. Paggi, A. Blazquez, A nonlinear finite thickness cohesive interface element for modeling delamination in fibre-reinforced composite laminates, Compo Part B-Eng, 109 (2017) 116-128. https://doi.org/10.1016/j.compositesb.2016.10.042

[22]. S. T. Nguyen, M. H. Vu, M. N. Vu, T. T. N. Nguyen, Generalized Maxwell model for micro-cracked viscoelastic materials, Int J Damage Mechs, 26 (2017) 697-710. https://doi.org/10.1177/1056789515608231

[23]. A. Rekik, T. T. N. Nguyen, A. Gasser, Coupling between homogenization techniques and brittle mechanics for modelling the behaviour of micro-cracked refractory linings, 14th Biennial Worldwide Congress UNITECR 2015, 2015 Sep, Vienne, Austria: Hal, 2016.

[24]. D. Lenczner, Creep and prestress losses in brick masonry, Struct Eng, 64 (1986), 57–62.

[25]. K. K. Choi, S. L. Lissel, M. M. Reda Taha, Rheological modelling of masonry creep, Can J Civil Eng, 34 (2007) 1506–1517. https://doi.org/10.1139/L07-06

[26]. S. T. Nguyen, L. Dormieux, Y. L. Pape, J. Sanahuja, A Burger model for the effective behavior of a microcracked viscoelastic solid, Int J Damage Mechs, 20 (2011) 1116-1129. https://doi.org/10.1177/1056789510395554

[27]. T. T. N. Nguyen, S. T. Nguyen, M. H. Vu, M. N. Vu, A. Gasser, A. Rekik, Effective viscoelastic properties of micro-cracked heterogeneous materials, Int J Damage Mechs, 25 (2016) 557-573. https://doi.org/10.1177/1056789515605557

[28]. A. Rekik, T. T. N. Nguyen, A. Gasser, Multi-level modeling of viscoelastic microcracked masonry, Int. J. Solids. Stru., 81 (2016) 63-83. https://doi.org/10.1016/j.ijsolstr.2015.11.002

[29]. S. T. Nguyen, Propagation de fissures et endommagement par microfissures des matériaux viscoélastiques linéaires non vieillissants, Université Paris-Est, 2010, PhD dissertation.

[30]. S. Ignoul, L. Schueremans, J. Tack, L. Swinnen, S. Feytons, L. Binda, D. V. Gemert, K. V. Balen, Creep behavior of masonry structures - failure prediction based on a rheological model and laboratory tests, Proceedings of the 5th int. seminar on Structural Analysis of Historical Constructions, 2006 Nov 6-8, Macmillan India, Lirias, 2006, 913-920.